INTERNATIONAL JOURNAL FOR NUMERICAL METHODS IN FLUIDS
Int. J. Numer. Meth. Fluids 2008; **58**:1327–1351
Published online 14 April 2008 in Wiley InterScience (www.interscience.wiley.com). DOI: 10.1002/fld.1787

Convergence of MPFA on triangulations and for Richards' equation

R. A. Klausen[1,*,†], F. A. Radu[2,‡] and G. T. Eigestad[3]

[1]*Centre of Mathematics for Applications, University of Oslo, Pb. 1053 Blindern, N-0316 Oslo, Norway*
[2]*Max-Planck Institute for Mathematics in the Sciences, Inselstr. 22, D-04103 Leipzig, Germany*
[3]*Centre for Integrated Petroleum Research, University of Bergen, Allegaten 41, N-5008, Bergen, Norway*

SUMMARY

Spatial discretization of transport and transformation processes in porous media requires techniques that handle general geometry, discontinuous coefficients and are locally mass conservative. Multi-point flux approximation (MPFA) methods are such techniques, and we will here discuss some formulations on triangular grids with further application to the nonlinear Richards equation. The MPFA methods will be rewritten to mixed form to derive stability conditions and error estimates. Several MPFA versions will be shown, and the versions will be discussed with respect to convergence, symmetry and robustness when the grids are rough. It will be shown that the behavior may be quite different for challenging cases of skewness and roughness of the simulation grids. Further, we apply the MPFA discretization approach for the Richards equation and derive new error estimates without extra regularity requirements. The analysis will be accompanied by numerical results for grids that are relevant for practical simulation. Copyright © 2008 John Wiley & Sons, Ltd.

Received 23 April 2007; Revised 23 November 2007; Accepted 15 January 2008

KEY WORDS: Richards' equation; error estimates; mixed finite element method; multi-point flux approximation

1. INTRODUCTION

Numerical simulation of transport and transformation processes in the subsurface has many application areas. Oil and gas production has played an important economic role over many years, and numerical modeling and simulation have helped in increasing the efficiency of exploiting these natural resources. The remediation of contaminated sites is another important application area for society and poses a challenge in highly industrialized and densely populated countries. Over the

*Correspondence to: R. A. Klausen, Center for Mathematics for Applications, University of Oslo, Pb. 1053 Blindern, N-0316 Oslo, Norway.
†E-mail: r.a.klausen@cma.uio.no
‡Present address: Helmholtz Center for Environmental Research-UFZ, Permoserstr. 15, D-04318 Leipzig, Germany.

past years, the technologies used in the oil and gas industry have received attention for possible sequestration of CO_2 to handle one issue associated with climate changes.

It is important to develop and apply simulation techniques for all of the above issues, and both a solid mathematical and a numerical foundations are crucial for forecasting of the physical processes.

Mathematically, the models in the above cases consist of nonlinear systems of parabolic differential equations, in general, of convection-dominated type. In the case of simulation of simultaneous flow of oil and water in porous media, the model of two phase flow is one of the core interests. The governing equations can be transformed by the concept of a global pressure [1] into a strongly coupled system of an elliptic equation and an (almost) hyperbolic equation.

In the case of contaminated sites, the modeling of the fluid transport constitutes the basis for the simulation. Although groundwater modeling (single phase flow) leads to linear elliptic problems, the consideration of the unsaturated soil results in the Richards equation ($1\frac{1}{2}$ phase flow) which is a nonlinear, degenerate elliptic–parabolic problem. Thus, in both these applications, linear elliptic boundary value problems result algorithmically as subproblems. Their numerical treatment is complicated by the porous medium properties: the natural variation of the conductivity is best described as rough and heterogeneous. This impacts both single phase modeling and modeling of the nonlinear equations that describe multi-phase flow in the porous medium. Regarding the embedding in the iterative solution of more complex problems, further requirements arise for the discretization methods: The methods should generate an explicit local velocity approximation as the essential driving force for coupled or subordinate transport process. The methods should also be locally mass conservative.

The sum of these requirements excludes classical finite difference methods and conformal finite element methods. Over the last years, intensive research has been done concerning alternative discretization methods that meet at least some of the above-mentioned requirements. These methods range from node-oriented finite volume (FV) methods, or cell-oriented FV, mixed finite element (MFE) methods and their variants with hybridization (HMFE) or extensions (EMFE) to discontinuous Galerkin methods. The multi-point flux approximation (MPFA) methods are cell-oriented FVMs that have been essentially developed and investigated in the last decade, cf. [2–9] among others. On the other hand, the HMFE method has been applied and investigated intensively for nonlinear degenerate elliptic–parabolic problems as the Richards equation cf. [10]. There is a close relationship between the two methods, cf. [6], where a convergence analysis is presented for MPFA on the basis of relations of this method to the MFE method [11]. A recent work [12] has investigated how a local mimetic finite difference method can be derived and relate this to MPFA methodology.

The convergence of the MFEM-scheme based on the Raviart–Thomas lowest-order elements for Richards' equation was analyzed in several papers [13–18]. Optimal order of convergence was obtained for the time continuous scheme in [13, 14]. Following the ideas there, an explicit order of convergence for the fully discrete scheme can be derived only by assuming extra regularity for the solution. In order to also cover the degenerate case, the techniques from [13] were combined with the one in [19] to obtain an explicit order of convergence for the MFEM scheme of Richards' equation in a general framework in [15]. The proof there is based on the equivalence between a conformal and a MFE schemes, at the continuous and semidiscrete level (time discrete). A further extension, which allows now a Hölder continuous saturation, was developed in [16].

However, a convergence proof for the numerical scheme based on MPFA and Euler implicit for the Richards equation is still missing. Here, we combine specific techniques for degenerate

DOI: 10.1002/fld

parabolic equations, MFE and MPFA discretizations to obtain a general convergence result for the fully discrete scheme. The order of convergence is given only in terms of the discretization parameters, i.e. the time step and the mesh diameter. The proof is done for both quadrilateral and triangular grids. The result is obtained without assuming unrealistic regularity for the solution of the Richards equation, which is the most important advantage of this approach.

The remainder of the paper is organized as follows: We first start with some basic assumptions for the theory discussed here. In Section 2, we discuss the use of the MPFA discretization on triangulations. Section 3 presents Richards' equation and contains the new theoretical error estimates when MPFA discretization is applied. Section 4 verifies the theoretical results for the MPFA discretization on triangular grids numerically and discusses limitations of the MPFA methods.

1.1. Basic assumptions

The groundwater movement, taking into account the unsaturated subregions near the surface, is described by the Richards equation, a nonlinear elliptic–parabolic partial differential equation:

$$\partial_t \Theta(\psi) - \nabla \cdot K(\Theta) \nabla(\psi + z) = 0 \quad \text{on } \Omega \times (0, T] \tag{1}$$

Here, $\Omega \subset \mathbb{R}^d$, $d = 1, 2, 3$, is bounded with a Lipschitz continuous boundary, ψ is the pressure head, Θ is the water content, K is the hydraulic conductivity and z is the height against the gravitational direction. The equation results from the mass conservation (volume conservation by assuming incompressibility of water) and Darcy's law.

In the presentation of the MPFA method, we will use as a prototype for the spatial variables of Richards' equation, or equivalently the pressure equation of fully multiphase flow system, cf. [20], the following elliptic equation:

$$-\operatorname{div}(\mathbf{K}(\mathbf{x}) \operatorname{grad} p) = g \quad \text{on } \Omega \tag{2}$$

with $\Omega \subset \mathbb{R}^2$ and boundary $\partial\Omega$, p denoting the pressure and $\mathbf{K}$ a possible heterogeneous and anisotropic conductivity tensor. The boundary condition is chosen for simplicity of exposition:

$$p(\mathbf{x}) = 0 \quad \text{on } \partial\Omega$$

Let $L^2(\Omega)$ be the space of square integrable functions on Ω and $H(\operatorname{div}, \Omega)$ the space of d-dimensional vector functions having the components and the divergence in $L^2(\Omega)$. We denote by $H^1(\Omega)$ the standard Sobolev spaces (see, e.g. [21]) and by $H^{-1}(\Omega)$ the dual space of $H_0^1(\Omega)$. The inner product $\langle \cdot, \cdot \rangle$ is the $L^2(\Omega)$-inner product or the duality pairing between $H_0^1(\Omega)$ and $H^{-1}(\Omega)$. Throughout this work, $\| \cdot \|$ denotes the norm in $L^2(\Omega)$ and $\| \cdot \|_1$ the norm in $H^1(\Omega)$. We use analogous notations for the inner product and the corresponding norm in $L^2(0, T; \mathscr{H})$, with $\mathscr{H}$ being either $L^2(\Omega)$, $H^1(\Omega)$ or $H^{-1}(\Omega)$. In addition, we often express u or $u(t)$ instead of $u(t, x)$ and use C to denote a generic positive constant, not depending on the discretization or regularization parameters.

Let $\{\mathscr{T}_h\}$ denote a family of regular triangulations on Ω, where h is the maximum element edge. Create a dual grid by dividing each cell into sub-cells given by the cell center and the edge midpoint, cf. Figure 1. Denote the dual grid, $\mathscr{I}_h$, where the dual cells, denoted interaction regions $I \in \mathscr{I}_h$, consist of the N sub-cells with a common vertex. Denote the sub-cells of I by E_i, with the inner sub-cell edges e_i, $i = 1, \ldots, N$. Finally, the set of all edges of $\mathscr{T}_h(\Omega)$ on Ω is denoted by $\mathscr{E}_h(\Omega)$.

DOI: 10.1002/fld

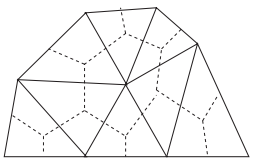

Figure 1. A triangulation, $\mathscr{T}_h$, and its dual grid, $\mathscr{I}_h$.

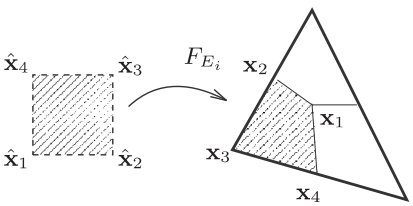

Figure 2. The reference mapping F_{E_i} from one unit square onto a sub-cell.

Note that the triangle sub-cells become general quadrilaterals. We construct a mapping F, from a unit square $\hat{E}$ onto each such quadrilateral sub-cell E_i, cf. Figure 2. Denote the vertex of each sub-cell $\mathbf{x}_i$, $i=1,2,3,4$, in the counter clockwise direction, and let $\mathbf{x}_1$ be the triangle center. If $\mathbf{x}_{ij}=(\mathbf{x}_i-\mathbf{x}_j)$ the transformation of the sub-cell is given by

$$F(\hat{x},\hat{y})=\mathbf{x}_1+\mathbf{x}_{21}\hat{x}+\mathbf{x}_{41}\hat{y}+(\mathbf{x}_{32}-\mathbf{x}_{41})\hat{x}\hat{y} \tag{3}$$

for $(\hat{x},\hat{y})\in\hat{E}$. The Jacobian matrix of F is denoted by $\mathbf{D}=\mathbf{D}_{E_i}$ and $J=J_{E_i}$ the absolute value of the Jacobian of the mapping.

2. THE MPFA

The MPFA discretization is a control volume formulation, where more than two pressure values are used in the spatial approximation across cell edges. The unknowns are the cell pressures and the half edge fluxes. The discretization is illustrated in Equation (2). The goal here is to define and illustrate the discretization principles and qualities of the method in a context as simple as possible. The spatial flux approximation is suited for approximation of the flux of Equation (1), as well as for a fully multiphase flow problem, cf. [20], as can be studied in, for instance, [2].

Here, we describe the method in a mixed form, which can also be formulated as a MFE method with broken Raviart–Thomas elements and a quadrature rule. The effect of the quadrature rule is decoupling of the MFE equations and results in a block diagonal mass matrix that easily can be inverted locally.

DOI: 10.1002/fld

2.1. MPFA as a MFE method

The MFE method that corresponds to MPFA as defined in, for instance, [3] can be expressed as $(\mathbf{q}_h, p_h) \in \mathscr{RT}_h^{1/2} \times W_h \subset H(\mathrm{div}, \Omega) \times L^2(\Omega)$ such that

$$\begin{aligned} a_h(\mathbf{q}_h, \mathbf{v}) - \langle p_h, \mathrm{div}\, \mathbf{v} \rangle = 0 \quad \text{for all } \mathbf{v} \in \mathscr{RT}_h^{1/2} \\ \langle \mathrm{div}\, \mathbf{q}_h, q \rangle = \langle g, q \rangle \quad \text{for all } q \in W_h \end{aligned} \tag{4}$$

The discrete space $W_h \subset L^2$ consists of cellwise constants, whereas we define the broken $\mathscr{RT}$-elements by splitting the usual triangular $\mathscr{RT}$-elements, cf. [22], from a three-dimensional to a six-dimensional space. For each edge e, we split the flux in two components, associated with each half edge. Then, let the new split element be linear in each half triangle, spanned by the midpoint of the actual edge and the opposite vertex, cf. Figure 3(a), and denote these functions $\mathscr{RT}^{1/2}$.

The corresponding finite element space, $\mathscr{RT}_h^{1/2}$ is still in $H(\mathrm{div}, \Omega)$, giving normal continuity also inside each triangle, and can be defined by

$$\mathscr{RT}_h^{1/2} := \left\{ \mathbf{v} \in H(\mathrm{div}, \Omega) : \mathbf{v}|_E \in \frac{1}{J} \mathbf{D}(\mathscr{RT}^{1/2}), \forall E \in \mathscr{T}_h \right\}$$

Hence, the canonical degrees of freedom for the space $\mathscr{RT}_h^{1/2}$ are $\mathbf{v} \cdot \mathbf{n}$ of each half edge in $\mathscr{E}_h^{1/2}$. If Π_h denotes the usual $\mathscr{RT}_h$-projection, cf. [22], the Brezzi condition applies only to the pair $(\Pi_h \mathscr{RT}_h^{1/2}, W_h)$. This corresponds to numerical tests where we see better behavior for the sum of the half edge fluxes, $\Pi_h \mathbf{q}_h$.

We define the quadrature rule similarly as for the quadrilateral case, cf. [6]. Let $v_k|_{e_{ik}} = v_{ik}$, which is the conserved value $\mathbf{v} \cdot \mathbf{n} = \hat{\mathbf{v}} \cdot \hat{\mathbf{n}}$ on the half edge e_{ik}, cf. Figure 3(b). Then

$$a_h(\mathbf{q}, \mathbf{v}) = \sum_{i=1}^{3} \sum_{j,k=1}^{2} \kappa_{jk}^{E_i} q_{ij} v_{ik} \tag{5}$$

for functions $\mathbf{v}, \mathbf{q}$ in $\mathscr{RT}_h^{1/2}$, and where κ_{jk} are components of Λ_{E_i}, to be defined next.

If

$$\left\langle J \mathbf{K}^{-1} \frac{1}{J} \mathbf{D}\hat{\mathbf{q}}, \frac{1}{J} \mathbf{D}\hat{\mathbf{v}} \right\rangle_{\hat{E}} = \langle \hat{\mathbf{K}}^{-1} \hat{\mathbf{q}}, \hat{\mathbf{v}} \rangle_{\hat{E}} \tag{6}$$

we have

$$\hat{\mathbf{K}}^{-1} = J^{-1} \mathbf{D}^{\mathrm{T}} \mathbf{K}^{-1} \mathbf{D} \tag{7}$$

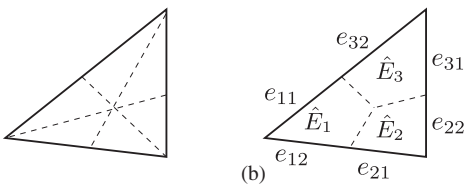

Figure 3. One cell split into six half triangles, (a), giving rise to, (b), three sub-cells $\hat{E}_i$ and the six half cell edges e_{ij}.

DOI: 10.1002/fld

On each sub-cell E_i, approximate $\hat{\mathbf{K}}^{-1}$ by the non-symmetric quantity

$$\Lambda_{E_i} = \frac{1}{J_{E_i}(\hat{\mathbf{x}}_3)} \mathbf{D}_{E_i}^{\mathrm{T}}(\hat{\mathbf{x}}_1) \mathbf{K}^{-1} \mathbf{D}_{E_i}(\hat{\mathbf{x}}_3) \tag{8}$$

Here, $\hat{\mathbf{x}}_1 = (0, 0)$ is the triangle center, whereas $\hat{\mathbf{x}}_3 = (1, 1)$ becomes the triangle vertex. The motivation for this approximation is given in the following section. Now, the quadrature rule in Equation (5) is then defined by the component, κ_{jk}, of Λ_{E_i}.

The quadrature rule Equation (5) can also be applied on the $\mathscr{BDM}_1$-elements, cf. [22]. The degrees of freedom for these elements are exactly the same as $\mathscr{RT}_h^{1/2}$. In this case, choose the degree of freedom associated with the two vertices of each edge; hence, $v_{ik} = v_k(\mathbf{x}_i)$, for $\mathbf{v} = (v_1, v_2)$.

2.2. Direct derivation of MPFA

Define a pressure space $P(I)$ on the interaction region I to be all linear on the sub-cells E_i, which are continuous on the boundary of I. For each $p \in P(I)$, let $\{p_k\}_{k=1,\ldots,N}$ be the values of p at the corners of I and $\{\lambda_k\}_{k=1,\ldots,N}$ the values of p at the continuity points, here the midpoints of the edges, see Figure 4.

The local pressure p is then uniquely defined by the $2N$ degrees of freedom $\{p_k, \lambda_k\}$. Let $\mathbf{K}_E$ be a cellwise constant approximation of $\mathbf{K}$. Along half edge e of sub-cell E_i, let

$$q_e|_{E_i} = -\mathbf{K}_E \operatorname{grad} p|_{E_i} \cdot \mathbf{n}_e \tag{9}$$

where $\mathbf{n}_e$ is the edge normal with $|\mathbf{n}_e| = |e|$. The MPFA pressure space, $P_{\mathrm{MPFA}}(I)$, is now further restricted to

$$P_{\mathrm{MPFA}}(I) = \{p \in P(I) : [q_e]_e = 0, \ \forall e \in \mathscr{E}^{1/2}(I)\} \tag{10}$$

where $\mathscr{E}^{1/2}(I)$ represents the four inner edges of I, $[\cdot]_e$ is the jump across edge e and q_e is defined by Equation (9). The uniqueness of $P_{\mathrm{MPFA}}(I)$ is shown in [6].

In a control volume formulation, the discretization lies in approximating the fluxes. This can now be characterized locally on each interaction region. Here, we define the MPFA in a mixed form, where the explicit flux expression is found after a local inversion on each interaction region. The approximation is based on linear pressure and constant velocities in each sub-cell. The degrees of freedom for linear pressure on each sub-cell are taken at the cell center and the two continuity

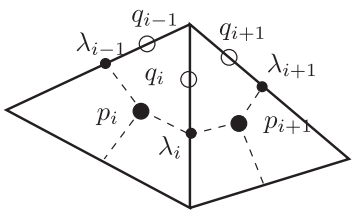

Figure 4. Two adjacent sub-cells. Let • denote the cell-centered pressures $\{p_i\}$, the small • the cell edge pressure $\{\lambda_i\}$ at the continuity points and ○ the edge velocities $\{q_i\}$ or edge flux.

DOI: 10.1002/fld

points on each edge. The continuity points may be chosen as the midpoints of the edges, but as we will see later this may impact on the discretization properties. From the linear pressure variation a constant gradient is found, based on the geometry of the sub-cell.

The normal component associated with a sub-cell E_i can be defined

$$[\mathbf{n}_1(\hat{x}), \mathbf{n}_2(\hat{y})] = \begin{bmatrix} y_{\hat{y}} & -y_{\hat{x}} \\ -x_{\hat{y}} & x_{\hat{x}} \end{bmatrix} = J\mathbf{D}^{-\mathrm{T}} \tag{11}$$

from Equation (3), where the inner sub-cell edge normal is found for $\hat{y}=0$ and $\hat{x}=0$, and the outer cell normal of the sub-cell is found for $\hat{y}=1$ and $\hat{x}=1$. The constant velocity is found from the linear pressure substituted into Equation (9), and

$$\begin{pmatrix} q_i \\ q_{i-1} \end{pmatrix} = \frac{1}{J(0,0)} [\mathbf{n}_1(1), \mathbf{n}_2(1)]^{\mathrm{T}} \mathbf{K} [\mathbf{n}_1(0), \mathbf{n}_2(0)] \begin{pmatrix} p_i - \lambda_i \\ p_i - \lambda_{i-1} \end{pmatrix} = \Lambda_{E_i}^{-1} \begin{pmatrix} p_i - \lambda_i \\ p_i - \lambda_{i-1} \end{pmatrix} \tag{12}$$

for sub-cell E_i, with edge e_i and e_{i-1}, cf. Figure 4. The cell center is always $\hat{\mathbf{x}}_1 = (0,0)$ for all sub-cells. The cell vertices are always $\hat{\mathbf{x}}_3 = (1,1)$ for all sub-cells. Therefore, inverting $\Lambda_{E_i}^{-1}$ gives Equation (8).

Let the components of Λ_{E_i} be denoted by κ_{jk}^i, for $j,k=1,2$. A similar expression on the adjacent sub-cell E_{i+1} makes elimination of the edge pressure λ_i possible. This gives the following expression associated with half edge e_i:

$$(\kappa_{11}^i + \kappa_{22}^{i+1}) q_i + \kappa_{12}^i q_{i-1} + \kappa_{21}^{i+1} q_{i+1} = p_{i+1} - p_i \tag{13}$$

This inverse formulation of MPFA can also be found in [5, 23]. By deriving the similar equations for the other interior edges of I, we obtain a $N \times N$ system of the form:

$$\mathbf{Aq} = \mathbf{Bp} \tag{14}$$

where the components of $\mathbf{Bp}$ are pressure differences, $\mathbf{q} = (q_1, \ldots, q_N)^{\mathrm{T}}$, and

$$\begin{pmatrix} (\kappa_{11}^1 + \kappa_{22}^2) & \kappa_{21}^2 & 0 & \cdots & \kappa_{12}^1 \\ \kappa_{12}^2 & (\kappa_{11}^2 + \kappa_{22}^3) & \kappa_{21}^3 & 0 & \cdots \\ 0 & \kappa_{12}^3 & (\kappa_{11}^3 + \kappa_{22}^4) & \kappa_{21}^4 & \\ \vdots & \vdots & & \ddots & \vdots \\ \kappa_{21}^1 & 0 & \cdots & \kappa_{12}^N & (\kappa_{11}^N + \kappa_{22}^1) \end{pmatrix} \tag{15}$$

Together with the control volume formula, or the second equation in (4), this gives a local system:

$$\begin{pmatrix} \mathbf{A} & \mathbf{B} \\ \mathbf{B}^{\mathrm{T}} & 0 \end{pmatrix} \begin{pmatrix} \mathbf{q} \\ -\mathbf{p} \end{pmatrix} = \begin{pmatrix} 0 \\ \mathbf{f} \end{pmatrix} \tag{16}$$

where we can solve for $\mathbf{B}^{\mathrm{T}}\mathbf{A}^{-1}\mathbf{Bp} = \mathbf{f}$ on each interaction region. The mixed system (16) is exactly the blocks corresponding to each dual cell from the MFE method (4). Note that unless the involved sub-cells are parallelograms, in which case Λ is symmetric, A is not symmetric. We, therefore,

DOI: 10.1002/fld

have to impose the stability criterion:

$$\det(\Lambda+\Lambda^{\mathrm{T}})>0 \tag{17}$$

This ensures the symmetric part of Λ to be positive definite.

2.3. MPFA variations

Above, the continuity point λ was given as the edge midpoints, cf. [24] which is standard. Analogously, the $\frac{1}{4}$ of each sub-cell edge can be used, as introduced by Edwards and Rogers [25]. The family of MPFA schemes with different continuity points was first presented in [4, 25], and a study for general structured/unstructured grids can be found in [7, 26].

In the case of edge midpoints, the discretization favors sub-cells that are close to or asymptotically approach squares or parallelograms, cf. [11, 27]. This is the case for quadrilateral grids, but is impossible to achieve for triangular grids. We now instead propose to divide the edges into $\frac{1}{3}$ parts and use the $\frac{1}{3}$ edge points as the two continuity points for each edge. The result is a symmetric MPFA method derived in physical space. This will take advantage of the simpler triangular cell shape compared with the quadrilateral cells.

We introduce the notation $C(\frac{1}{2})$, $C(\frac{1}{3})$ and $C(\frac{1}{4})$, for the different choices of continuity points, λ, on each half edge, where $C(\frac{1}{2})$ means the edge midpoint. The variational triangle spanned by p_i, λ_i and λ_{i-1}, illustrated in Figure 4, is used for approximation of the linear variation and is shown in Figure 5 for the different continuity points.

Unfortunately, the $C(\frac{1}{3})$ and $C(\frac{1}{4})$ methods do not by construction reduce to a two-point flux for the so-called $\mathbf{K}$-orthogonal grids, which is the case when $\hat{\mathbf{K}}$ from Equation (7) is diagonal. This means that the method does not reduce to the essential 1D finite difference method with harmonic mean in the case of essentially 1D flow across an edge with discontinuous conductivity. Extra tests are needed to recover two-point fluxes in such cases. On the other hand, no extra stability criteria such as (17) are needed for the $C(\frac{1}{3})$ version since the method is symmetric.

Lemma 1

The physical-space-based MPFA-$C(\frac{1}{3})$ methods are always symmetric and can be interpreted as a $\frac{3}{2}$-scaled reference-space-based method with vertex evaluation.

The physical-space-based MPFA-$C(\frac{1}{3})$ methods can also be interpreted as a MFE method with $\mathscr{BDM}_1$ elements.

Proof

The physical-space-based MPFA-$C(\frac{1}{3})$ methods can be described analogously to the description in Equation (12). The mapping F given by Equation (3) now goes onto the $\frac{1}{3}$ edge parallelogram

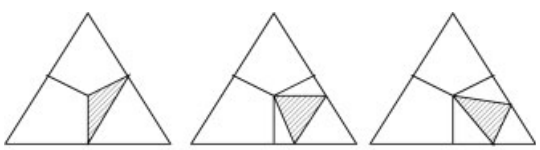

Figure 5. The variational triangle for $C(\frac{1}{2})$, $C(\frac{1}{3})$ and $C(\frac{1}{4})$.

DOI: 10.1002/fld

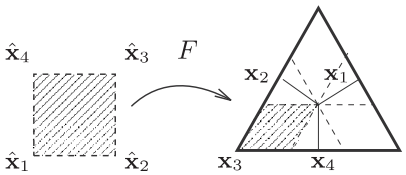

Figure 6. The scaled mapping for the physical space MPFA-$C(\frac{1}{3})$ methods.

shown in Figure 6, whereas we still use the full sub-cell edge normals. Let the superscript $C(\frac{1}{3})$ denote components associated with the $C(\frac{1}{3})$-parallelogram mapping. The analog to Equation (12) will then read

$$\begin{pmatrix} q_i \\ q_{i-1} \end{pmatrix} = \frac{1}{J^{C(1/3)}(0,0)} [\mathbf{n}_1(1), \mathbf{n}_2(1)]^{\mathrm{T}} \mathbf{K} [\mathbf{n}_1^{C(1/3)}(0), \mathbf{n}_2^{C(1/3)}(0)] \begin{pmatrix} p_i - \lambda_i \\ p_i - \lambda_{i-1} \end{pmatrix} \tag{18}$$

where $\mathbf{n}_i(1)$, $i=1,2$, is the same edge normal as used in Equation (12). The parallelogram has edges with length equal to $\frac{1}{3}$ of the full cell edge length; hence, $\mathbf{n}_i^{C(1/3)}(0) = \frac{2}{3}\mathbf{n}_i(1)$, $i=1,2$. Further $J^{C(1/3)}(0,0) = J^{C(1/3)}(1,1)$. Therefore,

$$\begin{aligned} &\frac{1}{J^{C(1/3)}(0,0)} [\mathbf{n}_1(1), \mathbf{n}_2(1)]^{\mathrm{T}} \mathbf{K} [\mathbf{n}_1^{C(1/3)}(0), \mathbf{n}_2^{C(1/3)}(0)] \\ &\quad = \frac{3/2}{J^{C(1/3)}(1,1)} [\mathbf{n}_1^{C(1/3)}(1), \mathbf{n}_2^{C(1/3)}(1)]^{\mathrm{T}} \mathbf{K} [\mathbf{n}_1^{C(1/3)}(1), \mathbf{n}_2^{C(1/3)}(1)] \\ &\quad = \frac{3}{2} \hat{\mathbf{K}}^{C(1/3)}(1,1) \end{aligned} \tag{19}$$

Also, note that $\hat{\mathbf{K}}^{C(1/3)}(1,1) = \hat{\mathbf{K}}(1,1)$, since the scaling of J is the square of that of $\mathbf{D}$. The physical-space-based MPFA-$C(\frac{1}{3})$ can now be described by (4), with κ_{jk} from Equation (5) given as elements of $2/3\hat{\mathbf{K}}^{-1}(1,1)$, on sub-cell E_i, instead of the non-symmetric evaluation given in Equation (8). The resulting methods are always symmetric since $\hat{\mathbf{K}}^{-1}(1,1)$ is symmetric. Denote the associated symmetric bilinear form $a_h^{C(1/3)}(\cdot,\cdot)$. This bilinear form can now be used on $\mathscr{BDM}_1$ elements with $v_{ik} = v_k(\mathbf{x}_i)$, for $\mathbf{v} = (v_1, v_2)$ and $\mathbf{x}_i$ the cell vertex of sub-cell E_i. □

To achieve the needed regularity for any analysis, the conductivity tensor $\mathbf{K}$ has to be smooth, whereas in practical simulations $\mathbf{K}$ will be a positive-definite constant tensor given for each cell. The approximation of smooth functions by cellwise constant values does not reduce any first-order approximation; therefore, the further presentation is built on the assumption that $\mathbf{K}$ has constant values on each cell and that the needed regularity is achieved.

The physical space MPFA-$C(\frac{1}{3})$ methods over triangular grids can be expressed as a perturbed MFE method with $\mathscr{BDM}_1$ elements, cf. Lemma 1. In this case, the perturbation of the MFE method is given by the perturbation $a_h^{C(1/3)}(\cdot,\cdot)$ of $a(\cdot,\cdot)$. The perturbation error here is given in Lemma 3. Note that on triangular element $\mathscr{RT}_0 \subset \mathscr{BDM}_1$, and also constant velocity fields, $P_0^2 \subset \mathscr{BDM}_1$. The lemma shows that the perturbed bilinear form is exact on uniform flow or constant velocity fields.

DOI: 10.1002/fld

Note that the mixed finite element methods with $\mathscr{BDM}_1$ elements described here are closely related to the multipoint MFE methods described in [9].

Lemma 2
Let $\mathbf{q}_0 \in P_0^2(E)$, $\mathbf{v} \in \mathscr{BDM}_1(E) = P_1^2(E)$, for all $E \in \mathscr{T}_h$. Then

$$a_h^{C(1/3)}(\mathbf{q}_0, \mathbf{v}) = a(\mathbf{q}_0, \mathbf{v})$$

Proof
On each sub-cell E_i, let $\mathbf{x}_i$ denote the cell vertex with $\hat{\mathbf{x}}_i = (1, 1)$. Then, cf. Equation (7), we have

$$\hat{\mathbf{K}}_{E_i}^{-1}(\hat{\mathbf{x}}_i) = J^{-1}(\hat{\mathbf{x}}_i)\mathbf{D}^{\mathrm{T}}(\hat{\mathbf{x}}_i)\mathbf{K}^{-1}\mathbf{D}(\hat{\mathbf{x}}_i)$$

Choose the degrees of freedom of the $\mathscr{BDM}_1$ elements such that

$$\mathbf{v}(\mathbf{x}_i) = \frac{1}{J^{C(1/3)}(\hat{\mathbf{x}}_i)}\mathbf{D}^{C(1/3)}(\hat{\mathbf{x}}_i)\tilde{\mathbf{v}}$$

for $\mathbf{v} \in \mathscr{BDM}_1$, and $\tilde{\mathbf{v}} = [v_{i1}, v_{i2}]^{\mathrm{T}}$ the discrete values on the sub-cell edges. From Equation (5),

$$\begin{aligned} a_h^{C(1/3)}(\mathbf{q}_0, \mathbf{v}) &= \sum_{i=1}^{3} \sum_{j,k=1} \kappa_{jk}^{E_i, C(1/3)} q_{ij} v_{ik} \\ &= \frac{3}{2} \sum_{i=1}^{3} \tilde{\mathbf{q}}_0^{\mathrm{T}} \hat{\mathbf{K}}_{E_i}^{-1}(\hat{\mathbf{x}}_i)\tilde{\mathbf{v}} \\ &= \frac{3}{2} \sum_{i=1}^{3} J^{C(1/3)}(\hat{\mathbf{x}}_i)\mathbf{q}_0^{\mathrm{T}}(\mathbf{x}_i)\mathbf{K}^{-1}\mathbf{v}(\mathbf{x}_i) \end{aligned} \tag{20}$$

Since

$$J^{C(1/3)}(\hat{\mathbf{x}}_i) = J^{C(1/3)}(1, 1) = |\mathbf{n}_1^{C(1/3)}(1) \times \mathbf{n}_2^{C(1/3)}(1)| = \tfrac{2}{3}|E_i| = \tfrac{2}{3}(\tfrac{1}{3}|E|)$$

we have

$$a_h^{C(1/3)}(\mathbf{q}_0, \mathbf{v}) = \sum_{i=1}^{3} \frac{|E|}{3}\mathbf{q}_0^{\mathrm{T}}\mathbf{K}^{-1}\mathbf{v}(\mathbf{x}_i) \tag{21}$$

Now $\mathbf{q}_0^{\mathrm{T}}\mathbf{K}^{-1}\mathbf{v} \in P_1^2(E)$ and the quadrature rule given in Equation (21) is exact on linear integrands so that

$$a_h^{C(1/3)}(\mathbf{q}_0, \mathbf{v}) = \int_E \mathbf{q}_0^{\mathrm{T}}\mathbf{K}^{-1}\mathbf{v}\,\mathrm{d}\mathbf{x} = a(\mathbf{q}_0, \mathbf{v}) \qquad \square$$

It is straightforward to show that $a_h^{C(1/3)}(\mathbf{v}, \mathbf{v})^{1/2}$ also is equivalent to the $\mathscr{L}_2$ norm on $\mathscr{BDM}_1$. This result means that there exist constants $\alpha_0, \alpha_1 > 0$, independent of h, such that

$$\alpha_0\|\mathbf{v}\|^2 \leqslant a_h^{C(1/3)}(\mathbf{v}, \mathbf{v}) \leqslant \alpha_1\|\mathbf{v}\|^2 \tag{22}$$

The following lemma controls the extra perturbations of the MFE method, which gives the MPFA-$C(\frac{1}{3})$ method.

DOI: 10.1002/fld

Lemma 3
Let $\mathbf{q} \in (H^1(\Omega))^2$, $\mathbf{v} \in \mathscr{BDM}_1$ and Π_h be the classical $\mathscr{RT}_0$-projection. Then there is a constant c, independent of h, such that

$$|a_h^{C(1/3)}(\Pi_h \mathbf{q}, \mathbf{v}) - a(\mathbf{q}, \mathbf{v})| \leqslant ch \|\mathbf{q}\|_1 \|\mathbf{v}\|$$

Proof
Let Π_0 be the $\mathscr{L}_2$-projection onto $P_0^2(E)$, cellwise constant vector functions. Then from Lemma 2, Equation (22) and classical interpolation results, cf. [22], we have

$$\begin{aligned} |a_h^{C(1/3)}(\Pi_h \mathbf{q}, \mathbf{v}) - a(\mathbf{q}, \mathbf{v})| &= a_h^{C(1/3)}((\Pi_h - \Pi_0)\mathbf{q}, \mathbf{v}) + a(\Pi_0 \mathbf{q} - \mathbf{q}, \mathbf{v}) \\ &\leqslant c(\|\Pi_h \mathbf{q} - \mathbf{q}\| + \|\Pi_0 \mathbf{q} - \mathbf{q}\|)\|\mathbf{v}\| \\ &\leqslant ch \|\mathbf{q}\|_1 \|\mathbf{v}\| \end{aligned}$$

□

An analog analysis to [6, 28] of a reference-space-based MPFA method-based $\mathscr{BDM}_1$ element is given in [9], with main focus on quadrilateral grids. Note that for quadrilateral grids, this method only converges for cells that asymptotically approach parallelogram cells, but the analysis does also apply to triangular grids.

3. RICHARDS' EQUATION

We now return to Richards' equation (1),

$$\partial_t \Theta(\psi) - \nabla \cdot K(\Theta) \nabla(\psi + z) = 0$$

from the introduction. For the two-coefficient functions, different models can be chosen to end up with a single unknown in (1). These are provided essentially by soil particularities and allow reducing all the unknowns in the above equation to a single unknown. For negative pressure values, the nonlinearities are monotonically non-decreasing. Therefore, (1) is a nonlinear parabolic equation there, but positive pressure values lead to a constant value of saturation and represent the region below the groundwater table, where the pressure obeys an elliptic equation. As a consequence, we deal with a nonlinear elliptic–parabolic equation whose solution is typically lacking regularity. Together with the high nonlinearities appearing in the coefficient functions, this makes the analysis of numerical schemes for problem (1) in general difficult. A classical trick to combine the two nonlinearities in (1) in just one is to apply the Kirchhoff transformation, as suggested in [29]:

$$\mathscr{K} : \mathbb{R} \longrightarrow \mathbb{R}, \quad \psi \longmapsto \int_0^{\psi} K(\Theta(s))\, \mathrm{d}s$$

Since $K(\Theta(s))$ is positive, this transformation can be inverted and Equation (1) can be rewritten in terms of a new variable, $p := \mathscr{K}(\psi)$. Now, defining

$$b(p) := \Theta \circ \mathscr{K}^{-1}(p), \quad k(b(p)) := K \circ \Theta \circ \mathscr{K}^{-1}(p) \tag{23}$$

and letting $\mathbf{e_z}$ denote the vertical unit vector, Equation (1) becomes

$$\partial_t b(p) - \nabla \cdot (\nabla p + k(b(p))\mathbf{e_z}) = 0 \quad \text{in } (0, T] \times \Omega \tag{24}$$

DOI: 10.1002/fld

By the above transformation, diffusion becomes linear in Equation (1). However, the problem may still remain degenerate, leading to solutions that lack regularity.

In what follows, we let Γ denote the boundary of the domain Ω. Let $J=(0,T]$ be a finite time interval. We are interested in solving (24) endowed with initial and boundary conditions:

$$\begin{aligned} \partial_t b(p)-\nabla\cdot(\nabla p+k(b(p))\mathbf{e_z})=0 \quad & \text{in } J\times\Omega \\ p=p^0 \quad & \text{in } 0\times\Omega \\ p=0 \quad & \text{on } J\times\Gamma \end{aligned} \tag{25}$$

Throughout this section, we make use of the following assumptions.

(A1) $\Omega\subset\mathbb{R}^d$ is bounded with Lipschitz continuous boundary.
(A2) $b\in C^1$ is non-decreasing and Lipschitz continuous.
(A3) $k(b(z))$ is continuous and bounded in z and satisfies, for all $z_1,z_2\in\mathbb{R}$, $|k(b(z_2))-k(b(z_1))|^2\leqslant C_k(b(z_2)-b(z_1))(z_2-z_1)$
(A4) $b(p^0)$ is essentially bounded (by 0 and 1) in Ω and $p^0\in L^2(\Omega)$.

Remark 1
Assumption (A2) can be replaced by a more general Hölder continuity, as done in [16].

A mixed formulation for problem (25) reads as follows.

Problem 1
Find $(p,\tilde{\mathbf{q}})\in L^2(J\times\Omega)\times X$ such that $b(p)\in L^\infty(J\times\Omega)$ and for all $t\in J$ the equations

$$\langle b(p(t))-b(p^0),w\rangle+\langle\nabla\cdot\tilde{\mathbf{q}}(\mathbf{t}),w\rangle=0 \tag{26}$$

$$\langle\tilde{\mathbf{q}}(\mathbf{t}),\mathbf{v}\rangle-\int_0^t\langle p(s),\nabla\mathbf{v}\rangle\,\mathrm{d}s+\int_0^t\langle k(b(p(s)))\mathbf{e_z},\mathbf{v}\rangle\,\mathrm{d}s=0 \tag{27}$$

hold for all $w\in L^2(\Omega)$ and $\mathbf{v}\in H(\mathrm{div},\Omega)$, with $X:=H^1(J;(L^2(\Omega))^d)\cap L^2(J;(H^1(\Omega))^d)$.

We proceed with the time discretization of Problem 1. The resulting scheme is equivalent with the Euler implicit scheme. Let $N>1$ be an integer giving the time step $\tau=T/N$. For a given $n\in\{1,2,\ldots,N\}$, with $t_n=n\tau$ we define the time discrete mixed variational problem.

Problem 2
Let $n\in\{1,\ldots,N\}$ and p^{n-1} be given. Find $(p^n,\mathbf{q^n})\in L^2(\Omega)\times H(\mathrm{div},\Omega)$ such that

$$\langle b(p^n)-b(p^0),w\rangle+\tau\left\langle\nabla\cdot\sum_{j=1}^{n}\mathbf{q^j},w\right\rangle=0 \tag{28}$$

$$a(\mathbf{q^n},\mathbf{v})-\langle p^n,\nabla\cdot\mathbf{v}\rangle+\langle k(b(p^n))\mathbf{e_z},\mathbf{v}\rangle=0 \tag{29}$$

for all $w\in L^2(\Omega)$, and $\mathbf{v}\in H(\mathrm{div},\Omega)$.

DOI: 10.1002/fld

3.1. Error estimates for the semidiscrete problem

The following result can be found in [15, Theorem 4.6, p. 1468].

Theorem 1
Assuming (A1)–(A4), if $(p, \tilde{\mathbf{q}})$ is the solution of Problem 1 and $(p^n, \mathbf{q}^{\mathbf{n}})$ solves Problem 2 ($n \in \{1, \ldots, N\}$), we have

$$\sum_{n=1}^{N} \int_{t_{n-1}}^{t_n} \langle b(p(t)) - b(p^n), p(t) - p^n \rangle \, \mathrm{d}t + \left\| \sum_{n=1}^{N} \int_{t_{n-1}}^{t_n} (p(t) - p^n) \, \mathrm{d}t \right\|_1^2 + \left\| \tilde{\mathbf{q}}(\mathbf{T}) - \tau \sum_{n=1}^{N} \mathbf{q}^{\mathbf{n}} \right\|^2 \leqslant C\tau$$

where C does not depend on the time step τ.

Remark 2
Using the Lipschitz continuity of $b(\cdot)$ together with the above estimates, we can immediately obtain an error estimate for the saturation:

$$\sum_{n=1}^{N} \int_{t_{n-1}}^{t_n} \| b(p(t)) - b(p^n) \|^2 \, \mathrm{d}t \leqslant C\tau$$

3.2. Error estimates for the fully discrete problem

We have already presented error estimates for the semidiscrete scheme, we continue by giving estimates for the case semidiscrete to discrete. In the end of the section, we then conclude with a convergence result for the fully discrete MPFA scheme for the Richards equation. We distinguish the two cases of quadrilateral and triangular grids. In the first case, the fully discrete scheme is based on the broken Raviart–Thomas space, whereas in the second one the discrete variational formulations is based on the $\mathscr{BDM}_1$ space. Following [3], we have that MPFA for quadrilaterals is equivalent with the MFE method defined as follows.

Problem 3Q
Let $n \in \{1, \ldots, N\}$. Find $(p_h^n, \mathbf{q}_\mathbf{h}^\mathbf{n}) \in W_h \times \mathscr{RT}_h^{1/2}$ such that

$$\langle b(p_h^n), w_h \rangle + \tau \left\langle \sum_{j=1}^{n} \nabla \cdot \mathbf{q}_\mathbf{h}^\mathbf{j}, w_h \right\rangle = \langle b(p_h^0), w_h \rangle \tag{30}$$

$$a_h(\mathbf{q}_\mathbf{h}^\mathbf{n}, \mathbf{v_h}) - \langle p_h^n, \nabla \cdot \mathbf{v_h} \rangle + a_h(k(b(p_h^n))\mathbf{e_z}, \mathbf{v_h}) = 0 \tag{31}$$

for all $w_h \in W_h$ and $\mathbf{v_h} \in \mathscr{RT}_h^{1/2}$.

In the case of triangles, as described in Section 2.3, we come to the following MFE discrete formulation.

DOI: 10.1002/fld

Problem 3T
Let $n \in \{1, \ldots, N\}$. Find $(p_h^n, \mathbf{q_h^n}) \in W_h \times \mathscr{BDM}_1$ such that

$$\langle b(p_h^n), w_h \rangle + \tau \left\langle \sum_{j=1}^{n} \nabla \cdot \mathbf{q_h^j}, w_h \right\rangle = \langle b(p_h^0), w_h \rangle \tag{32}$$

$$a_h^{C(1/3)}(\mathbf{q_h^n}, \mathbf{v_h}) - \langle p_h^n, \nabla \cdot \mathbf{v_h} \rangle + a_h^{C(1/3)}(k(b(p_h^n))\mathbf{e_z}, \mathbf{v_h}) = 0 \tag{33}$$

for all $w_h \in W_h$ and $\mathbf{v_h} \in \mathscr{BDM}_1$.

For clarity, in the following section we recapitulate the basic estimates, which have been proved in [3] and Section 2.3. These estimates will be used to prove the convergence of MPFA schemes applied to Richards' equation. We first present error estimates for the case of quadrilateral grids. The triangular case is much easier to prove, and the result is given as a remark, without a complete proof.

3.3. Basic estimates

For the physical space MPFA-$C(\frac{1}{2})$ methods over quadrilateral grids, the following two lemmas can be found in [6].

Lemma 4
For all $\mathbf{v_h} \in \mathscr{RT}_h^{1/2}$ and $w_h \in W_h$, there holds

$$a_h(w_h, \mathbf{v_h} - \Pi_h \mathbf{v_h}) = 0 \tag{34}$$

From which the following lemma follows.

Lemma 5
Let $\mathbf{q} \in (H^1(\Omega))^2$, $\mathbf{v} \in \mathscr{RT}_h^{1/2}$, and Π_h is the classical $\mathscr{RT}_0$-projection, cf. [22]. Then there is a constant c, independent of h, such that

$$|a_h(\Pi_h \mathbf{q}, (I - \Pi_h)\mathbf{v})| \leqslant ch \|\mathbf{q}\|_1 \|(I - \Pi_h)\mathbf{v}\|$$

The following lemma is the equivalent of Lemma 3, Section 2.3, for the case of triangular grids.

Lemma 6
Let $\mathbf{q} \in (H^1(\Omega))^2$, $\mathbf{v} \in \mathscr{RT}_h$ and Π_h is the classical $\mathscr{RT}_0$-projection, cf. [22]. Then there is a constant c, independent of h, such that

$$|a_h(\Pi_h \mathbf{q}, \mathbf{v}) - a(\mathbf{q}, \mathbf{v})| \leqslant ch \|\mathbf{q}\|_1 \|\mathbf{v}\|$$

Important for our analysis are also the estimates:

$$\begin{aligned} &\alpha_m \|\mathbf{v_h}\|^2 \leqslant a_h(\mathbf{v_h}, \mathbf{v_h}) \leqslant \alpha_M \|\mathbf{v_h}\|^2 \quad \forall \mathbf{v_h} \in \mathscr{RT}_h^{1/2} \\ &\alpha_m \|\mathbf{v_h}\|^2 \leqslant a_h^{C(1/3)}(\mathbf{v_h}, \mathbf{v_h}) \leqslant \alpha_M \|\mathbf{v_h}\|^2 \quad \forall \mathbf{v_h} \in \mathscr{BDM}_1 \end{aligned} \tag{35}$$

3.4. Error estimates in the case of quadrilateral grids

Expressing MPFA as a perturbed MFEM, the perturbation can be divided into two steps. First a splitting of the classical Raviart–Thomas elements into $\mathscr{RT}_h^{1/2}$, and finally a quadrature rule is

DOI: 10.1002/fld

applied to the bilinear form. To control these perturbations, two basic lemmas are used, cf. [6]. This first lemma controls the accuracy of the splitting, and the second lemma controls the accuracy of the quadrature rule, cf. Lemmas 5 and 6. The following results are obtained by combining the techniques in [6] with the one in [15].

Theorem 2
Let $n \in \{1, \ldots, N\}$, and assume that (A1)–(A4) hold. If $(p^n, \mathbf{q^n})$ solves Problem 2 and $(p_h^n, \mathbf{q_h^n})$ is the solution of Problem 3Q, then there holds

$$\tau \sum_{n=1}^{N} \langle b(p^n) - b(p_h^n), p^n - p_h^n \rangle + \tau^2 \left\| \sum_{n=1}^{N} (\Pi_h \mathbf{q^n} - \mathbf{q_h^n}) \right\|^2$$

$$\leqslant Ch^2 \sum_{n=1}^{N} (\tau \|\mathbf{q^n}\|_1^2 + \tau \|p^n\|_1^2) \tag{36}$$

Proof
We will give the proof just for the case without convection, for an easier understanding of the ideas. The same techniques would also be used in the case with convection and, additionally, one will make use of Lemma 4 and the continuity of $a_h(\cdot, \cdot)$. We begin by introducing the notation:

$$\mathbf{e_q^n} = \sum_{j=1}^{n} (\Pi_h \mathbf{q^j} - \mathbf{q_h^j}) \in \mathscr{RT}_h^{1/2}$$

By subtracting Equations (30) and (31) from (28) and (29), respectively, we obtain

$$\langle b(p^n) - b(p_h^n), w_h \rangle + \tau \left\langle \nabla \cdot \sum_{j=1}^{n} \Pi_h (\mathbf{q^j} - \mathbf{q_h^j}), w_h \right\rangle = 0 \tag{37}$$

$$a(\mathbf{q^n}, \mathbf{v_h}) - a_h(\mathbf{q_h^n}, \mathbf{v_h}) + \langle p^n - p_h^n, \nabla \cdot \mathbf{v_h} \rangle = 0 \tag{38}$$

for all $w_h \in W_h$ and $\mathbf{v_h} \in \mathscr{RT}_h^{1/2}$. The operator Π_h here denotes the classical $\mathscr{RT}_0$-projection.

From (38), it also follows that

$$a(\mathbf{q^n}, \mathbf{v_h}) - a_h(\mathbf{q_h^n}, \mathbf{v_h}) + \langle P_h p^n - p_h^n, \nabla \cdot \mathbf{v_h} \rangle = 0 \tag{39}$$

for all $\mathbf{v_h} \in \mathscr{RT}_h$. P_h here denotes the usual L^2-projection, see, e.g. [15].

Now taking $\mathbf{v_h} = \tau \sum_{j=1}^{n} \Pi_h (\mathbf{q^j} - \mathbf{q_h^j}) \in \mathscr{RT}_h \subset \mathscr{RT}_h^{1/2}$, $w_h = P_h p^n - p_h^n$ in (39) and (37), respectively, and summing up the result from $n = 1$ to N, we obtain

$$\sum_{n=1}^{N} \langle b(p^n) - b(p_h^n), P_h p^n - p_h^n \rangle + \sum_{n=1}^{N} \tau a \left(\mathbf{q^n}, \sum_{j=1}^{n} \Pi_h (\mathbf{q^j} - \mathbf{q_h^j}) \right)$$

$$- \sum_{n=1}^{N} \tau a_h \left(\mathbf{q_h^n}, \sum_{j=1}^{n} \Pi_h (\mathbf{q^j} - \mathbf{q_h^j}) \right) = 0 \tag{40}$$

DOI: 10.1002/fld

or equivalently

$$T_1+\sum_{n=1}^{N}\tau\left(a\left(\mathbf{q^n},\sum_{j=1}^{n}\Pi_h(\mathbf{q^j}-\mathbf{q_h^j})\right)-a_h\left(\Pi_h\mathbf{q^n},\sum_{j=1}^{n}\Pi_h(\mathbf{q^j}-\mathbf{q_h^j})\right)\right)$$

$$+\sum_{n=1}^{N}\tau a_h\left(\Pi_h\mathbf{q^n}-\mathbf{q_h^n},\sum_{j=1}^{n}\Pi_h(\mathbf{q^j}-\mathbf{q_h^j})\right)=0\ \Leftrightarrow\ T_1+T_{21}+T_{22}=0 \tag{41}$$

We estimate now each of the terms above separately:

$$T_1=\sum_{n=1}^{N}\langle b(p^n)-b(p_h^n),p^n-p_h^n\rangle+\sum_{n=1}^{N}\langle b(p^n)-b(p_h^n),P_hp^n-p^n\rangle=:T_{11}+T_{12} \tag{42}$$

For T_{11}, using the Lipschitz continuity of $b(\cdot)$, there holds

$$T_{11}\geqslant\frac{1}{2}\sum_{n=1}^{N}\langle b(p^n)-b(p_h^n),p^n-p_h^n\rangle+C\sum_{n=1}^{N}\|b(p^n)-b(p_h^n)\|^2 \tag{43}$$

Applying the inequality $ab\leqslant\delta_1a^2/2+b^2/(2\delta_1)$, where $\delta_1>0$, T_{12} reads

$$|T_{12}|\leqslant\frac{\delta_1}{2}\sum_{n=1}^{N}\|b(p^n)-b(p_h^n)\|^2+\frac{1}{2\delta_1}\sum_{n=1}^{N}\|P_hp^n-p^n\|^2 \tag{44}$$

for all $\delta_1>0$. Using Lemma 6 and

$$\|\Pi_h\mathbf{v}\|\leqslant C\|\mathbf{v}\|\quad\forall\mathbf{v}\in\mathscr{R}\mathscr{T}_h^{1/2} \tag{45}$$

we obtain for T_{21}:

$$T_{21}\leqslant C\sum_{n=1}^{N}\tau h\|\mathbf{q^n}\|_1\|\Pi_h\mathbf{e_q^n}\|\leqslant C_1\sum_{n=1}^{N}\tau h\|\mathbf{q^n}\|_1\|\mathbf{e_q^n}\|\leqslant\sum_{n=1}^{N}\frac{h^2}{2\delta_2}\|\mathbf{q^n}\|_1^2+\frac{C_2\delta_2}{2}\sum_{n=1}^{N}\tau^2\|\mathbf{e_q^n}\|^2 \tag{46}$$

We now proceed by estimating T_{22},

$$T_{22}=\sum_{n=1}^{N}\tau a_h\left(\Pi_h\mathbf{q^n}-\mathbf{q_h^n},\sum_{j=1}^{n}\Pi_h\mathbf{q^j}-\mathbf{q_h^j}\right)+\sum_{n=1}^{N}\tau a_h\left(\Pi_h\mathbf{q^n}-\mathbf{q_h^n},\sum_{j=1}^{n}(\mathbf{q_h^j}-\Pi_h\mathbf{q_h^j})\right)$$

$$=T_{221}+\sum_{n=1}^{N}\tau a_h\left(\Pi_h\mathbf{q^n},\sum_{j=1}^{n}(\mathbf{q_h^j}-\Pi_h\mathbf{q_h^j})\right)-\sum_{n=1}^{N}\tau a_h\left(\mathbf{q_h^n},\sum_{j=1}^{n}(\mathbf{q_h^j}-\Pi_h\mathbf{q_h^j})\right) \tag{47}$$

$$=T_{221}+T_{2221}+T_{2222} \tag{48}$$

Further, there holds

$$T_{221}=\frac{\tau}{2}a_h(\mathbf{e_q^N},\mathbf{e_q^N})+\frac{\tau}{2}\sum_{n=1}^{N}a_h(\Pi_h\mathbf{q^n}-\mathbf{q_h^n},\Pi_h\mathbf{q^n}-\mathbf{q_h^n})$$

$$\geqslant C\tau\|\mathbf{e_q^N}\|^2+C\tau\sum_{n=1}^{N}\|\Pi_h\mathbf{q^n}-\mathbf{q_h^n}\|^2 \tag{49}$$

DOI: 10.1002/fld

To estimate the term T_{2221}, we make use of Lemma 5 and inequality (45). It follows

$$T_{2221} \leqslant C \sum_{n=1}^{N} \tau h \|\mathbf{q}^{\mathbf{n}}\|_1 \left\| \sum_{j=1}^{n} (\mathbf{q}_{\mathbf{h}}^{\mathbf{j}} - \Pi_h \mathbf{q}_{\mathbf{h}}^{\mathbf{j}}) \right\|$$

$$\leqslant C_1 \sum_{n=1}^{N} \tau h \|\mathbf{q}^{\mathbf{n}}\|_1 \|\mathbf{e}_{\mathbf{q}}^{\mathbf{n}}\|$$

$$\leqslant C_1 \sum_{n=1}^{N} h^2 \|\mathbf{q}^{\mathbf{n}}\|_1^2 + C_1 \sum_{n=1}^{N} \tau^2 \|\mathbf{e}_{\mathbf{q}}^{\mathbf{n}}\|^2 \tag{50}$$

We now use Equation (31) (we recall that we considered the case without convection) to show that $T_{2222} = 0$:

$$T_{2222} = -\sum_{n=1}^{N} \tau a_h \left(\mathbf{q}_{\mathbf{h}}^{\mathbf{n}}, \sum_{j=1}^{n} (\mathbf{q}_{\mathbf{h}}^{\mathbf{j}} - \Pi_h \mathbf{q}_{\mathbf{h}}^{\mathbf{j}}) \right)$$

$$= -\tau \left\langle p_h^n, \nabla \cdot \sum_{j=1}^{n} (\mathbf{q}_{\mathbf{h}}^{\mathbf{j}} - \Pi_h \mathbf{q}_{\mathbf{h}}^{\mathbf{j}}) \right\rangle = 0 \tag{51}$$

From (41)–(51), choosing δ_1 properly and using the discrete Gronwall Lemma we obtain the result. □

We have obtained above an estimate for the flux variable. To also obtain an upper bound for the error in the pressure, we recall the following result (see [30] for the proof).

Lemma 7
Assuming (A1) and given a $f_h \in W_h$, a $\mathbf{v_h} \in \mathscr{RT}_h$ exists such that

$$\nabla \cdot \mathbf{v_h} = f_h \quad \text{and} \quad \|\mathbf{v_h}\| \leqslant C \|\nabla \cdot \mathbf{v_h}\|$$

with $C > 0$ being a constant not depending on h, f_h or $\mathbf{v_h}$.

For the Raviart–Thomas finite elements, the following theorem can be found in [15]. We again adapt the proof for the case of a MPFA scheme.

Theorem 3
Let $n \in \{1, \ldots, N\}$ and assume that (A1)–(A4) hold. If $(p^n, \mathbf{q}^{\mathbf{n}})$ solves Problem 2 and $(p_h^n, \mathbf{q}_{\mathbf{h}}^{\mathbf{n}})$ is the solution of Problem 3Q, then there holds

$$\tau \left\| \sum_{n=1}^{N} (P_h p^n - p_h^n) \right\|^2 \leqslant C h^2 \sum_{n=1}^{N} (\|\mathbf{q}^{\mathbf{n}}\|_1^2 + \|p^n\|_1^2) \tag{52}$$

Proof
Again, we consider the case without convection, the extension to the general case being but straightforward. By summing up Equation (39) form $n = 1$ to N, we obtain

$$a \left(\sum_{n=1}^{N} \mathbf{q}^{\mathbf{n}}, \mathbf{v_h} \right) - a_h \left(\sum_{n=1}^{N} \mathbf{q}_{\mathbf{h}}^{\mathbf{n}}, \mathbf{v_h} \right) + \left\langle \sum_{n=1}^{N} (P_h p^n - p_h^n), \nabla \cdot \mathbf{v_h} \right\rangle = 0 \tag{53}$$

DOI: 10.1002/fld

for all $\mathbf{v_h} \in \mathscr{RT}_h$. By making use of Lemma 7, there exists $\mathbf{v_h} \in \mathscr{RT}_h$ such that $\nabla \cdot \mathbf{v_h} = \sum_{n=1}^{N} (P_h p^n - p_h^n)$ and

$$\|\mathbf{v_h}\| \leqslant C \|\nabla \cdot \mathbf{v_h}\| = C \left\| \sum_{n=1}^{N} (P_h p^n - p_h^n) \right\| \tag{54}$$

Introducing this $\mathbf{v_h}$ in (53), we obtain

$$\begin{aligned} \left\| \sum_{n=1}^{N} (P_h p^n - p_h^n) \right\|^2 &= a\left(\sum_{n=1}^{N} \mathbf{q^n}, \mathbf{v_h} \right) - a_h\left(\sum_{n=1}^{N} \Pi_h \mathbf{q^n}, \mathbf{v_h} \right) + a_h\left(\sum_{n=1}^{N} (\Pi_h \mathbf{q^n} - \mathbf{q_h^n}), \mathbf{v_h} \right) \\ &= T_1 + T_2 \end{aligned} \tag{55}$$

We proceed by estimating now the terms T_1 and T_2 separately. By using Lemma 6 and estimate (54), we obtain for the first term:

$$\begin{aligned} T_1 &\leqslant Ch \left\| \sum_{n=1}^{N} \mathbf{q^n} \right\|_1 \|\mathbf{v_h}\| \\ &\leqslant \frac{Ch^2}{2\delta_1} \left\| \sum_{n=1}^{N} \mathbf{q^n} \right\|_1^2 + \frac{\delta_1}{2} \|\mathbf{v_h}\|^2 \\ &\leqslant \frac{Ch^2}{2\delta_1 \tau} \sum_{n=1}^{N} \|\mathbf{q^n}\|_1^2 + \frac{C\delta_1}{2} \left\| \sum_{n=1}^{N} (P_h p^n - p_h^n) \right\|^2 \end{aligned} \tag{56}$$

with $\delta_1 > 0$ arbitrarily. For the second term in (55), we use the continuity of $a_h(\cdot,\cdot)$. There holds

$$\begin{aligned} T_2 &\leqslant C \left\| \sum_{n=1}^{N} (\Pi_h \mathbf{q^n} - \mathbf{q_h^n}) \right\| \|\mathbf{v_h}\| \\ &\leqslant \frac{C}{2\delta_2} \left\| \sum_{n=1}^{N} (\Pi_h \mathbf{q^n} - \mathbf{q_h^n}) \right\|^2 + \frac{\delta_2}{2} \|\mathbf{v_h}\|^2 \\ &\leqslant \frac{C}{2\delta_2} \left\| \sum_{n=1}^{N} (\Pi_h \mathbf{q^n} - \mathbf{q_h^n}) \right\|^2 + \frac{C\delta_2}{2} \left\| \sum_{n=1}^{N} (P_h p^n - p_h^n) \right\|^2 \end{aligned} \tag{57}$$

for all $\delta_2 > 0$. Now using also Theorem 2 and choosing δ_1 and δ_2 properly, one obtains from (55)–(57) result (52). □

The general convergence result can now be given for quadrilateral grids. One more assumption is needed:

(A5) $\mathbf{q^n} \in H^1(\Omega)^d$ for all $n \in \{1, \ldots, N\}$.

Assumption (A5) is in the 1D case evidently satisfied, because there $H(\mathrm{div}, \Omega) = H^1(\Omega)$. It also holds in the multidimensional case if $\partial\Omega$ is smooth enough and $k(\cdot)$ is differentiable (see [15]). By now combining the results obtained in Theorems 1–3 and using stability estimates for Problem 2 (as in [15, 16]), we obtain the following theorem.

DOI: 10.1002/fld

Theorem 4
Assuming (A1)–(A5) true, if $(p, \tilde{\mathbf{q}})$ is the solution of Problem 1 and $(p_h^n, \mathbf{q}_\mathbf{h}^\mathbf{n})$ solves Problem 3Q for all $n \in \{1, \ldots, N\}$, then there holds

$$\left\| \sum_{n=1}^{N} \int_{t_{n-1}}^{t_n} (p(t) - p_h^n)\, \mathrm{d}t \right\|^2 + \left\| \tilde{\mathbf{q}}(\mathbf{T}) - \tau \sum_{n=1}^{N} \mathbf{q}_\mathbf{h}^\mathbf{n} \right\|^2 \leqslant C(\tau + h^2) \tag{58}$$

Remark 3
An optimal order of convergence $(\tau^2 + h^2)$ can be shown by assuming extra regularity for the solution (see [15, 16]). More general estimates, with an order of convergence depending on the Hölder continuity of $b(\cdot)$, can be obtained by using the ideas in [16].

Remark 4
The same convergence results also hold for triangular grids. In this case, the proof of Theorem 2 follows immediately by using Lemma 3 and the ideas in [15, Proposition 4.10, p. 1470]. The proof is much easier in this case because the MFE scheme is defined by using $\mathscr{BDM}_1$ elements and not by the broken Raviart–Thomas space. This implies that the $\nabla \cdot \mathbf{v}_\mathbf{h} \in W_h$, for $\mathbf{v}_\mathbf{h} \in \mathscr{BDM}_1$, and the only quantity that has to be fixed is

$$|a_h^{C(1/3)}(\Pi_h \mathbf{q}, \mathbf{v}) - a(\mathbf{q}, \mathbf{v})|$$

This is handled by Lemma 3. Further, the proofs of Theorems 2 and 4 are absolutely similar.

Remark 5
In both the case of quadrilaterals and triangles, the grid is assumed to be regular enough to satisfy the technical lemmas necessary in the work with the used projectors.

4. NUMERICAL RESULTS

Next, we present numerical results for the various version of MPFA discretization on triangular control volumes illustrated in Equation (2). The triangular grids that we use are generated from underlying quadrilaterals, and we will test how the methods perform on various degrees of skewness, anisotropy and grid aspect ratios. As mentioned above, there is a choice for continuity points in the interaction region, cf. Section 2.3. If the MPFA-$C(\frac{1}{3})$ method is used, the resulting coefficient matrix is symmetric, whereas the standard midpoint method, $C(\frac{1}{2})$, does in general not yield symmetry.

Figure 7 shows a typical example of the rough grids that are used here, and for which convergence of Equation (2) is studied. Here, all corners of a uniform grid are perturbed randomly by a factor up to 70% of the associated triangle edge length. The grid is further stretched by a factor 100 in the x-direction. Note that a stretching of the simulation domain corresponds to medium anisotropy on a non-stretched domain.

We will here focus on the properties of the possible discretization schemes and differences between them. The main differences are utilized by simple homogeneous permeability problems. For numerical examples with discontinuous coefficient problems (for the $C(\frac{1}{2})$ scheme), refer to Bause and Hoffmann [31] for a more detailed study.

DOI: 10.1002/fld

In the numerical study below, we test the different MPFA triangle methods on various grids for solutions of Equation (2). The error of the pressure p is measured by $\|p_h - p(\mathbf{x}_c)\|$, where $\mathbf{x}_c$ is the triangle centroid, whereas the error of the velocity $\mathbf{q}$ is measured by the discrete norm:

$$\|\mathbf{q}-\mathbf{q}_h\|_h^2 = \sum_{E\in\mathcal{T}_h}\sum_{e\in E}(\mathbf{q}(\mathbf{x}_e)\cdot\mathbf{n}_e - q_e)^2|E|/3$$

where $\mathbf{x}_e$ is the midpoint of edge e.

4.1. Discretization in physical space

Our first tests are on grids similar to the ones visualized in Figure 8, where the triangulation either yields acute or non-acute angles. These grids are perturbations of the same order as the grid cell size of underlying uniform triangulations on parallelogram domains and will be referred to as rough grids, cf. [6]. The 'acute' triangulations describe a more regular family of grids, cf. [32] and, therefore, seems the most appropriate and robust for the discretization. For the homogeneous cases we test here, we will use the analytical solution of Equation (2):

$$\cosh(\pi x/\sqrt{k_x})\cos(\pi y/\sqrt{k_y}) \tag{59}$$

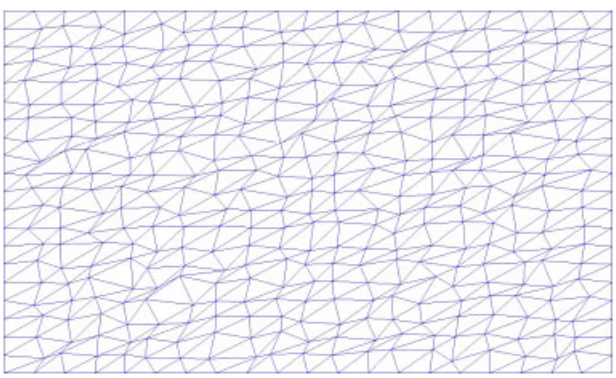

Figure 7. Example of rough triangulation of $[0,1]\times[0,0.01]$ on which Equation (2) is solved.

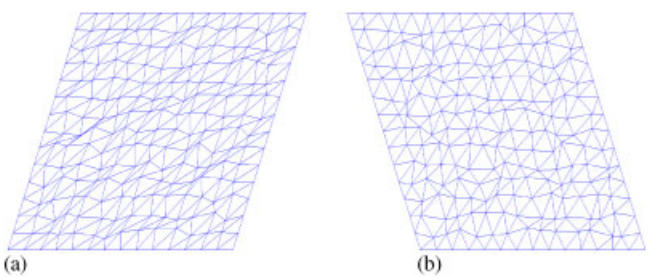

Figure 8. Various triangulations with perturbations: (a) predominantly non-acute angles and (b) predominantly acute angles.

DOI: 10.1002/fld

which represents divergence-free flow on a homogeneous medium with anisotropic conductivity

$$\mathbf{K}=\begin{bmatrix} k_x & 0 \\ 0 & k_y \end{bmatrix} \tag{60}$$

We first use parallelogram domains where the height and width have unit length, the medium is isotropic, and the grids are $n \times n$. The skewness of the domain is $\pi/3$, and the triangulation is either acute or non-acute as in Figure 8. For uniform grid refinements on either of these domains, the convergence is second order for both pressure and normal velocities in the discrete L^2-norm. These convergence rates are the same as the ones observed for the MPFA O-method on uniformly refined quadrilateral grids, cf. [27]. In Figures 9 and 10, we have plotted the convergence behavior for $n \times n$ grids where the grids are perturbed randomly by the same order as the grid cell size. As seen from these figures, the observed convergence rates for the pressure for both the discrete L^2- and L^∞-norms are close to second order, whereas the L^2-errors of the normal velocities seem to converge by order h^1. This is again in accordance with the rates observed in [27] for rough grids. The max errors for the normal velocities seem to converge by an order smaller than h^1; this may be more apparent for the non-acute triangulation. (The analytical pressure solution is different on the two different parallelogram domains, so that the error level is not directly comparable.)

In Figure 11, we have plotted the corresponding results for the symmetric $C(\frac{1}{3})$ method in physical space for the triangulation that yields triangles with predominantly acute angles. As seen from the plot, the convergence behavior is similar to the discretization that uses midpoints of edges as potential continuity points, but note the fact that the errors are here significantly smaller for the symmetric method.

Next, we test the convergence behavior on a parallelogram domain, where the grid aspect ratio is gradually increased. It has been observed that the combination of rough grids and large grid aspect

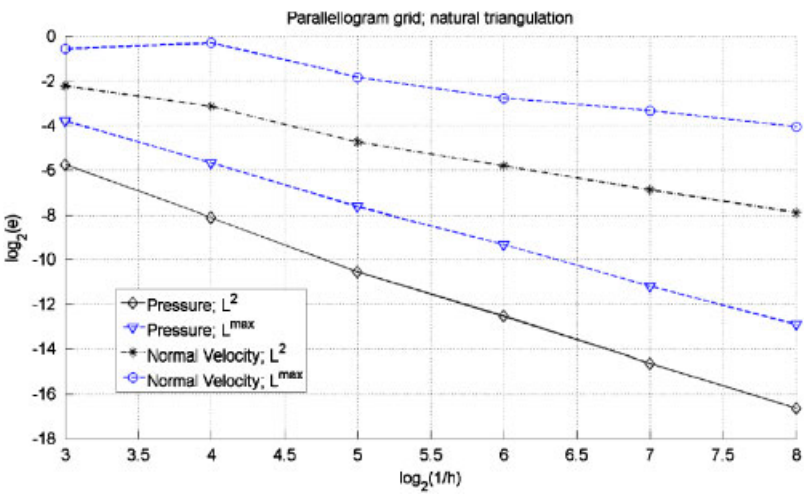

Figure 9. Convergence for rough triangular grids: acute triangulation. Second-order convergence seen for pressure and first order for normal velocities in discrete L^2-norm. Roughly, first-order convergence observed in L^∞-norm.

DOI: 10.1002/fld

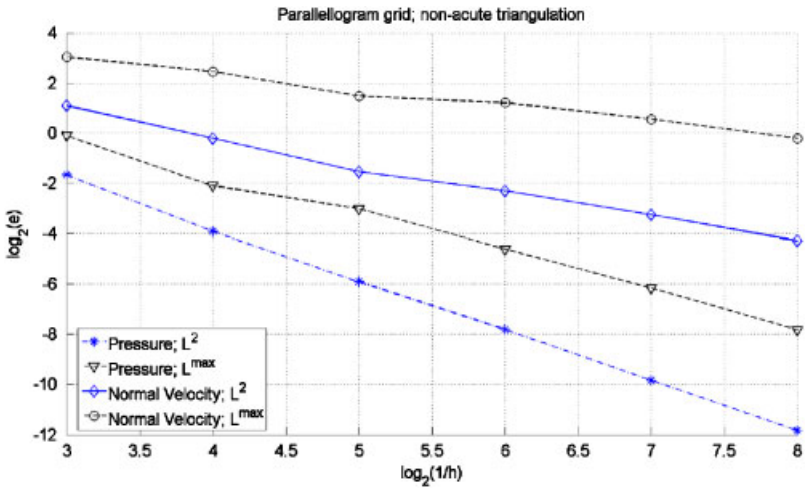

Figure 10. Convergence for rough triangular grids: non-acute triangulation. Almost second-order convergence seen for pressure and first order for normal velocities in discrete L^2-norm. Convergence rates in L^∞ somewhat smaller than first order.

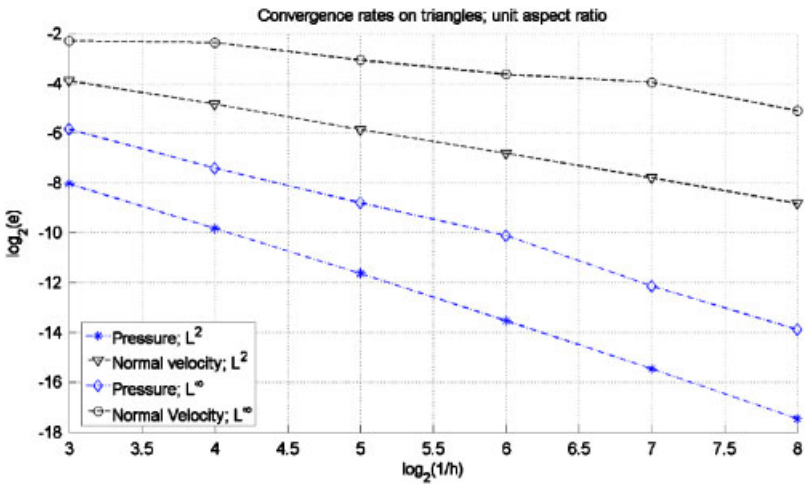

Figure 11. Convergence behavior for symmetriced discretization on triangles. Angles are mostly acute after grid perturbations; second-order convergence is observed for pressure and first order is observed for normal velocities in L^2-norm.

ratios leads to either the loss of convergence or diminished convergence rate for the O-method on quadrilaterals (in physical space), cf. [33] for details. This has initiated alternative methods that seek to reduce the number of cells that contributes to the flux stencils. The L-method introduced in [33] seems to have much better convergence properties for rough grids, but monotonicity problems

DOI: 10.1002/fld

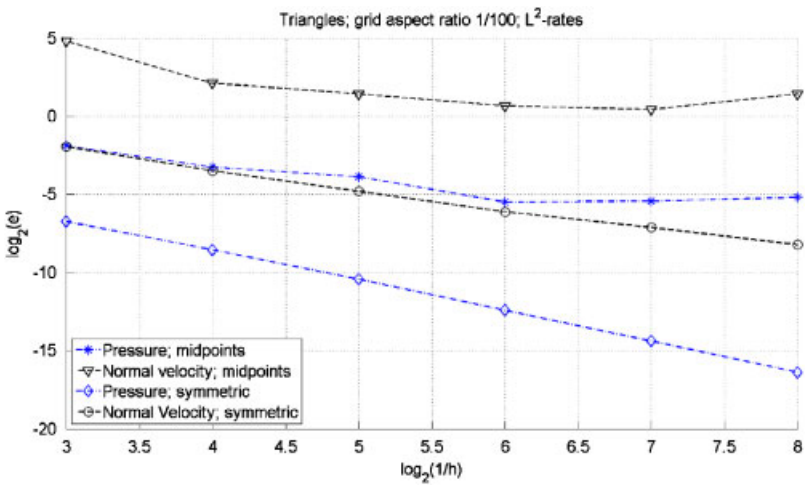

Figure 12. Convergence for the non-symmetric and symmetric methods in physical space for grid aspect ratios of $\frac{1}{100}$. Only the symmetric method can be claimed to be convergent.

may still cause unwanted behavior. Note that both the O- and L-methods in physical space are in general non-symmetric.

The MPFA O-method on triangular grids yields larger cell and flux stencils than the O-method on quadrilaterals. The cell stencils from the grid in Figure 8 will in general contain up to 13 cells, and this could potentially cause problems with stability. In Figure 12, we have shown the convergence behavior for the MPFA-$C(\frac{1}{2})$ method (which is un-symmetric) on a $\pi/3$ parallelogram domain where the medium is compressed by a factor $\frac{1}{100}$ in the y-direction. As seen from the plot, the error may behave fairly arbitrary from grid refinement to grid refinement, and it seems like the method is not asymptotically convergent. Note, however, the trend of decreasing errors for the initial refinements. For the symmetric MPFA-$C(\frac{1}{3})$ method, the situation is completely different. Although the discretization on triangles yields larger cell and flux stencils, the underlying symmetry of the method has such a 'strong' effect that the discretization is now convergent. Both the pressure and normal velocities converge; in particular, second-order convergence for the pressure and first order for the normal velocities seem to be retained for the errors in discrete L^2-norm. This is indeed superior behavior compared with the O-method on quadrilateral grids for the same grid aspect ratios, where convergence cannot be established!

4.1.1. Comments on discretization in reference space. In Section 2.3 and Lemma 1, we describe the symmetric physical space MPFA-$C(\frac{1}{3})$ method by a transformation of the domain to a reference space. The reference space method is easy to implement via transformations of sub-cell conductivity to unit squares. The reference space method is then convergent for all cases tested above. This is again different from the behavior for the reference space method on quadrilaterals, where convergence is lost for rough grids, and convergence may only be obtained for uniform grid refinement.

In conclusion, the MPFA O-method on triangles has the potential to be symmetriced without loosing convergence. Symmetry is obtained either through a smart choice of continuity point along

DOI: 10.1002/fld

Table I. Order of asymptotic pressure convergence for various MPFA methods.

Rough grids	Unit aspect ratio	$\frac{1}{100}$ aspect ratio
MPFA-$C(\frac{1}{2})$	$O(h^2)$	$O(1)$
MPFA-$C(\frac{1}{3})$	$O(h^2)$	$O(h^2)$

the flux edge ($\frac{1}{3}$-points) in physical space or by making a transformation to computational space. The methods are linked by Lemma 1. When large grid aspect ratios are introduced, convergence seems to be retained, making the method superior compared with the O-method on quadrilateral grids. The convergence properties of the methods are summarized in Table I.

ACKNOWLEDGEMENTS

We would like to thank Prof. Ivar Aavatsmark, Prof. Peter Knabner and Joachim Hoffmann for the valuable discussions and input related to this work.

REFERENCES

1. Chavent G, Jaffré J. *Mathematical Models and Finite Elements for Reservoir Simulation*. North-Holland: Amsterdam, 1986.
2. Aavatsmark I. An introduction to multipoint flux approximations for quadrilateral grids. *Computational Geosciences* 2002; **6**:404–432.
3. Aavatsmark I, Barkve T, Bøe Ø, Mannseth T. Discretization on non-orthogonal, quadrilateral grids for inhomogeneous, anisotropic media. *Journal of Computational Physics* 1996; **127**:2–14.
4. Edwards MG, Rogers CF. Finite volume discretization with imposed flux continuity for the general tensor pressure equation. *Computational Geosciences* 1998; **2**:259–290.
5. Edwards MG. Unstructured, control-volume distributed, full-tensor finite-volume schemes with flow based grids. *Computational Geosciences* 2002; **6**:433–452.
6. Klausen RA, Winther R. Robust convergence of multi point flux approximation on rough grids. *Numerische Mathematik* 2006; **104**:317–337.
7. Pal M, Edwards MG, Lamb AR. Convergence study of a family of flux-continuous finite-volume schemes for the general tensor pressure equation. *International Journal for Numerical Methods in Fluids* 2006; **51**:1177–1203.
8. Vohralik M. Equivalence between mixed finite element and multi-point finite volume methods. *Comptes Rendus de l'Académie des Sciences* (*Paris*) *Series I* 2004; **339**:525–528.
9. Wheeler MF, Yotov I. A multipoint flux mixed finite element method. *SIAM Journal on Numerical Analysis* 2006; **44**:2082–2106.
10. Knabner P, Schneid E. Adaptive hybrid mixed finite element discretization of instationary variably saturated flow in porous media. In *High Performance Scientific and Engineering Computing*, Breuer M *et al.* (eds). Springer: Berlin, 2002; 37–44.
11. Klausen RA, Russell TF. Relationships among some locally conservative discretization methods which handle discontinuous coefficients. *Computational Geosciences* 2004; **8**:341–377.
12. Lipnikov K, Shashkov M, Yotov I. Local flux mimetic finite difference methods. *Technical Report TR-MATH 05-13*, University of Pittsburgh, 2006.
13. Arbogast T, Wheeler MF, Zhang NY. A nonlinear mixed finite element method for a degenerate parabolic equation arising in flow in porous media. *SIAM Journal on Numerical Analysis* 1996; **33**:1669–1687.
14. Schneid E, Knabner P, Radu FA. A priori error estimates for a mixed finite element discretization of the Richards' equation. *Numerische Mathematik* 2004; **98**:353–370.
15. Radu FA, Pop IS, Knabner P. Order of convergence estimates for an Euler implicit, mixed finite element discretization of Richards' equation. *SIAM Journal on Numerical Analysis* 2004; **42**:1452–1478.

DOI: 10.1002/fld

16. Radu FA, Pop IS, Knabner P. Error estimates for a mixed finite element discretization of some degenerate parabolic equations. *Numerische Mathematik*. DOI: 10.1007/s00211-008-0139-9.
17. Bause M. Higher and lowest order mixed finite element approximation of subsurface flow problems with solutions of weak regularity. *Advanced in Water Resources*, 2007. DOI:10.1016/j.advwatres.2007.09.003.
18. Woodward C, Dawson C. Analysis of expanded mixed finite element methods for a nonlinear parabolic equation modeling flow into variably saturated porous media. *SIAM Journal on Numerical Analysis* 2000; **37**:701–724.
19. Nochetto RH, Verdi C. Approximation of degenerate parabolic problems using numerical integration. *SIAM Journal on Numerical Analysis* 1988; **25**:784–814.
20. Aziz K, Settari A. *Petroleum Reservoir Simulation*. Elsevier: London, 1979.
21. Adams RA. *Sobolev Spaces*. Academic Press: New York, 1975.
22. Brezzi F, Fortin M. *Mixed and Hybrid Finite Element Methods*. Springer: New York, 1991.
23. Aavatsmark I, Barkve T, Mannseth T. Control-volume discretization methods for 3D quadrilateral grids in inhomogeneous, anisotropic reservoirs. *SPE Journal* 1998; **3**:146–154.
24. Aavatsmark I, Barkve T, Bøe Ø, Mannseth T. Discretization on unstructured grids for inhomogeneous, anisotropic media. Part I: derivation of the methods. Part II: discussion and numerical results. *SIAM Journal on Scientific Computing* 1998; **19**:1700–1736.
25. Edwards MG, Rogers CF. A flux continuous scheme for the full tensor pressure equation. In *Proceedings of the 4th European Conference on the Mathematics of Oil Recovery*, Røros, Norway, Chrsitie MA, Farmer CL, Heinemann ZE (eds), 1994.
26. Edwards MG. M-matrix flux splitting for general tensor discretization operators on structured and unstructured grids. *Journal of Computational Physics* 2000; **160**:1–28.
27. Aavatsmark I, Eigestad GT, Klausen RA. *Numerical Convergence of MPFA for General Quadrilateral Grids in Two and Three Dimensions*. IMA Volumes in Mathematics and Its Applications, vol. 142. Compatible spatial discretizations, Springer: 2006; 1–22.
28. Klausen RA, Winther R. Convergence of multi point flux approximations on quadrilateral grids. *Numerical Methods for Partial Differential Equations* 2006; **22**:1438–1454.
29. Alt HW, Luckhaus S. Quasilinear elliptic–parabolic differential equations. *Mathematische Zeitschrift* 1983; **183**:311–341.
30. Thomas JM. Sur l'analyse numérique des méthodes d'éléments finis hybrides et mixtes. *Thése d'Etat*, Université Pierre & Marie Curie (Paris 6), 1977.
31. Bause M, Hoffmann J. A comparative study of mixed finite element and multi point flux approximations of flows in porous media. *Proceedings of ENUMATH*, 2007.
32. Ciarlet PG. *The Finite Element Method for Elliptic Problem*. North-Holland: Amsterdam, 1978.
33. Aavatsmark I, Eigestad GT, Mallison BT, Nordbotten JM. A compact multipoint flux approximation method with improved robustness. *Numerical Methods for Partial Differential Equations*. DOI: 10.1002/num.20320.